Simulations of heat transport in singlemolecule junctions: Investigations of the thermal diode effect

Cite as: J. Chem. Phys. 157, 174105 (2022); https://doi.org/10.1063/5.0125714

Submitted: 13 September 2022 • Accepted: 14 October 2022 • Accepted Manuscript Online: 14 October 2022 • Published Online: 03 November 2022

Jonathan J. Wang, Jie Gong, D Alan J. H. McGaughey, et al.







ARTICLES YOU MAY BE INTERESTED IN

Quantum mechanics of open systems: Dissipaton theories

The Journal of Chemical Physics 157, 170901 (2022); https://doi.org/10.1063/5.0123999

Coupled charge and energy transfer dynamics in light harvesting complexes from a hybrid hierarchical equations of motion approach

The Journal of Chemical Physics 157, 174104 (2022); https://doi.org/10.1063/5.0117659

The Wigner localization of interacting electrons in a one-dimensional harmonic potential The Journal of Chemical Physics 157, 174107 (2022); https://doi.org/10.1063/5.0112413

The Journal of Chemical Physics Special Topics Open for Submissions



Simulations of heat transport in single-molecule junctions: Investigations of the thermal diode effect

Cite as: J. Chem. Phys. 157, 174105 (2022); doi: 10.1063/5.0125714 Submitted: 13 September 2022 • Accepted: 14 October 2022 • **Published Online: 3 November 2022**







Jonathan J. Wang, Jie Gong, Alan J. H. McGaughey, Dand Dvira Segal J. 3, a)





AFFILIATIONS

- ¹Chemical Physics Theory Group, Department of Chemistry, University of Toronto, 80 Saint George St., Toronto, Ontario M5S 3H6, Canada
- ² Department of Mechanical Engineering, Carnegie Mellon University, Pittsburgh, Pennsylvania 15213, USA
- Department of Physics, University of Toronto, 60 Saint George St., Toronto, Ontario M5S 1A7, Canada

ABSTRACT

With the objective of understanding microscopic principles governing thermal energy flow in nanojunctions, we study phononic heat transport through metal-molecule-metal junctions using classical molecular dynamics (MD) simulations. Considering a single-molecule gold-alkanedithiol-gold junction, we first focus on aspects of method development and compare two techniques for calculating thermal conductance: (i) The Reverse Nonequilibrium MD (RNEMD) method, where heat is inputted and extracted at a constant rate from opposite metals. In this case, the thermal conductance is calculated from the nonequilibrium temperature profile that is created at the junction. (ii) The Approach-to-Equilibrium MD (AEMD) method, with the thermal conductance of the junction obtained from the equilibration dynamics of the metals. In both methods, simulations of alkane chains of a growing size display an approximate length-independence of the thermal conductance, with calculated values matching computational and experimental studies. The RNEMD and AEMD methods offer different insights, and we discuss their benefits and shortcomings. Assessing the potential application of molecular junctions as thermal diodes, alkane junctions are made spatially asymmetric by modifying their contact regions with the bulk, either by using distinct endgroups or by replacing one of the Au contacts with Ag. Anharmonicity is built into the system within the molecular force-field. We find that, while the temperature profile strongly varies (compared with the gold-alkanedithiol-gold junctions) due to these structural modifications, the thermal diode effect is inconsequential in these systems—unless one goes to very large thermal biases. This finding suggests that one should seek molecules with considerable internal anharmonic effects for developing nonlinear thermal devices.

Published under an exclusive license by AIP Publishing. https://doi.org/10.1063/5.0125714

I. INTRODUCTION

The function, performance, and stability of electronic, plasmonic, thermal, and thermoelectric devices fundamentally rely on their heat conduction properties and energy dissipation pathways.¹⁻⁹ Unlike electrons, which are directly controlled by electrostatic and electromagnetic fields, phonons, the quanta of vibrational energy, are not feasibly manipulated by external driving forces. Can we control and direct vibrational energy flow at the nanoscale, down to the level of a single molecule? Before addressing this question, we must first understand the relationship between molecular structure and the ensuing thermal transport properties.

Recent studies of phononic heat conduction in single-molecule junctions were focused on quasi one-dimensional (1D) organic molecules. Specifically, since alkane chains are poor conductors of charge carriers, one can safely assume that their thermal conductance is dominated by their nuclear motion and neglect the contribution of electrons. Phononic thermal transport in alkane chains of 2-10 repeating units (and sometimes longer) was simulated in Refs. 10-17 with different techniques (classical or quantum) and varying degree of details (one-dimensional or three-dimensional models, explicit metals, or Langevin baths), with measurements reported in Refs. 18 and 19. Experimental studies were also performed on self-assembled monolayers (SAMs) of alkane

^{a)}Author to whom correspondence should be addressed: dvira.segal@utoronto.ca

molecules^{20–25} with atomistic simulations reported in Refs. 24–29. Both single-molecule and SAM junctions were generally shown to support ballistic (non-dissipative) heat transport that was approximately length-independent in long enough chains (typically beyond 10 units). Given their simple structure and the ensuing ballistic thermal behavior, alkane chains serve as a testbed for developing computational methodologies for single-molecule phonon heat transport.

Toward the long-term objective of deciphering the structure-function question in phonon heat flow at the nanoscale, in this study we focus on two objectives: (i) method development and benchmarking of computational techniques, (ii) modeling and simulations of nonlinear thermal devices, specifically single-molecule thermal diodes. Considering alkane-based junctions, we focus on the atomistic contribution to thermal energy transport, also referred to as phononic heat transport (in the bulk, which is the source of thermal energy in our work, the phonon description is valid). Compared with quantum calculations, ^{30,31} classical molecular dynamics (MD) simulations can feasibly include anharmonic interactions, which could be influential in molecules at high temperatures. Moreover, for Au-alkane-Au nanojunctions, it was found that quantum statistics played a small role around room temperatures, ¹⁶ justifying simulations based on classical MD.

We perform atomistic-classical nonequilibrium MD simulations of Au-alkanedithiol-Au junctions and related-modified systems using the Large-scale Atomic/Molecular Massively Parallel Simulator (LAMMPS)³² and study their thermal conduction as a function of length, temperature bias, and contact properties. The first part of the paper, Sec. II is devoted to aspects of method development and benchmarking. Here, our objective is to find what (possibly complementary) microscopic information different computational techniques convey, their benefits, and shortcomings. We utilize two methodologies for extracting the phonon conductance of molecular junctions: In the first method, which we discuss in Sec. II A, we implement reverse nonequilibrium molecular dynamics (RNEMD) simulations. Here, kinetic energy is added to one Au lead, and removed from the other side, both at a constant rate. In response, a temperature gradient develops across the junction, allowing us to calculate the thermal conductance of the junction. This method was previously implemented to, e.g., describe heat conduction in a silicon-polyethylene-silicon single-molecule junction¹¹ and in Au-SAM-Au systems.^{24–26} The second method, discussed in Sec. II B is referred to as the approach-to-equilibrium molecular dynamics (AEMD) method. This tool was recently applied to investigate the thermal resistance of molecular junctions based on ab initio quantum dynamics.³³ In this approach, the thermal conductance is determined from the equilibration dynamics of the bulk metals by monitoring their changing temperatures. In Sec. II C, thermal conductances obtained from these two computational approaches are compared with other studies and to experiments and discussed.

Continuing to applications, the main nontrivial question that we probe in the subsequent Sec. III is whether an alkane-based junction could materialize the thermal diode effect by making it spatially asymmetric through modifications to its boundaries. Thermal diodes are devices that conduct heat asymmetrically upon reversal of the temperature bias. 34–38 Based on minimal models, see, e.g., Refs. 39 and 40, it was argued that a diode effect can be generated at the nanoscale when two conditions are met: The junction is

spatially asymmetric and effects are at play. We incorporate asymmetry in two distinct ways: (i) We modify one of the endgroups to enhance asymmetry, as well as anharmonicity. (ii) We build junctions with mismatched metal contacts. In both cases, anharmonicity is included in the force-field. Our analysis reveals that while the temperature profile generated in the molecule is sensitive to spatial asymmetry, the ensuing thermal diode effect is insignificant in alkane-based junctions unless the temperature bias is made very large ($T_h - T_c > 200$ K, with $T_{h,c}$ the temperatures of the opposite metals). Section IV brings predictions on the linear conductance of homogeneous and mismatched junctions. We summarize our work in Sec. V, further suggesting directions for future work.

II. SIMULATION TECHNIQUES

We discuss here the two simulation methods that we implemented and tested for studying thermal conductance with LAMMPS: The reverse nonequilibrium MD, which is based on steady-state simulations, and the approach-to-equilibrium MD, which relies on transient dynamics.

A. Reverse nonequilibrium molecular dynamics

The RNEMD method employs a reverse procedure for determining the current-thermal bias (or specifically the thermal conductance), compared with the direct nonequilibrium MD method. ^{15–17,26–29,41} In RNEMD, one equilibrates the total system to a certain temperature (300 K in this work), then imposes the heat current as a parameter. In turn, the temperature profile in the junction is obtained in the nonequilibrium steady-state limit. The heat current is given by the rate of adding (extracting) kinetic energy into (from) atoms in the hot (cold) baths. By splitting the system into sections, a temperature profile resultant of the energy flow is obtained by calculating the kinetic energy on sections of the metals and the molecule.

We define the temperature bias on the junction as $\Delta T_{\mathrm{M-M'}}$, with M=Au, Ag identifying the metal contact; the temperatures are evaluated on the metal, but close to the molecule. We also characterize an *intrinsic molecular* temperature difference, which is defined between the two endgroups. In an alkanedithiol junction, this temperature bias is measured S-to-S, $\Delta T_{\mathrm{S-S}}$. We illustrate these two temperature differences in Fig. 1.

These biases are used for the determination of two thermal conductance values, $G_{\rm M-M'}$ and $G_{\rm S-S}$, based on the linear response expression,

$$G = \frac{J}{\Delta T}. (1)$$

 $G_{\mathrm{M-M'}}$ corresponds to experimental measurements of thermal conductance in molecular junctions, ^{18,19} since then, temperatures are practically measured at the metal contacts. In contrast, while $G_{\mathrm{S-S}}$ is affected by the molecule being hybridized to the metal contacts, it provides deeper insights into the thermal transport behavior within the molecule itself.

We present in Fig. 1 a graphical representation of the junction and its partition into sections (a), the resultant nonequilibrium temperature profile under a certain value of the heat current J (b), and a demonstration of the approximately linear relationship between

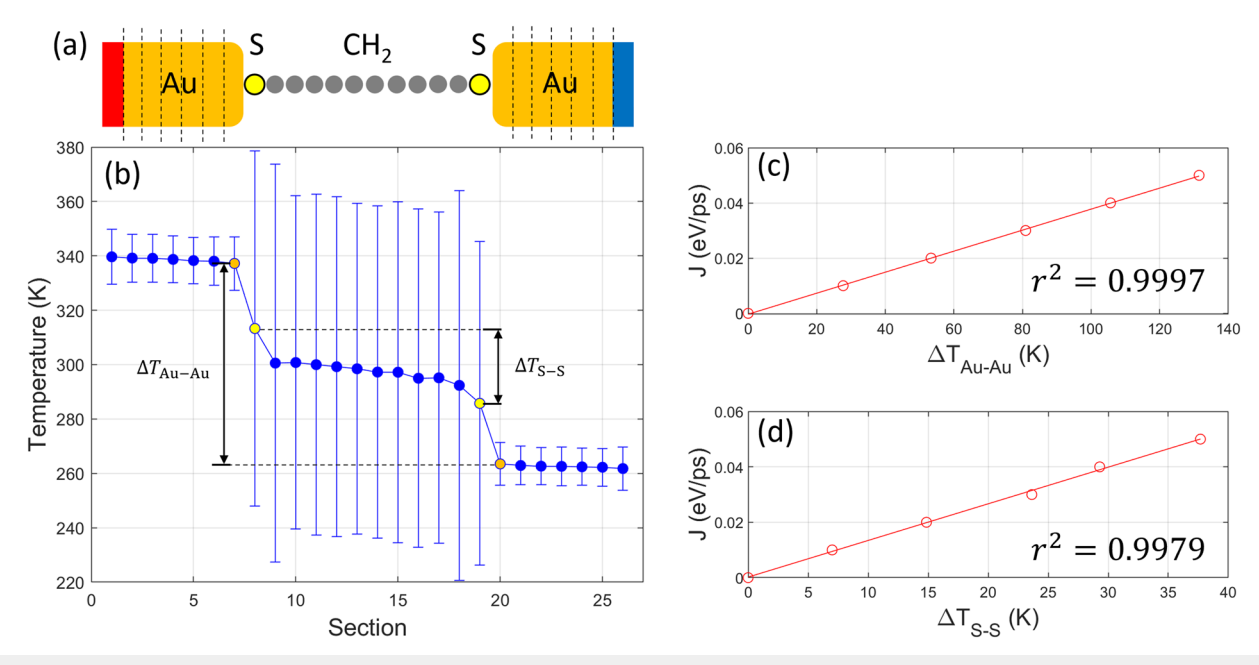


FIG. 1. Simulation results from the RNEMD method. (a) A graphical representation of a single-molecule junction; regions in the metals over which the temperature is evaluated are separated by dashed lines. (b) The temperature profile obtained in RNEMD simulations, shown for $N_C = 10$ under the heat current J = 0.02 eV/ps. Each data point represents a time-averaged temperature of Au sections and individual atoms in the chain as displayed in (a). We define two temperature biases, ΔT_{Au-Au} and ΔT_{S-S} evaluated as the difference between either gold or yellow data points, respectively. (c) and (d) Imposed heat current against the resulting temperature bias (c) ΔT_{Au-Au} and (d) ΔT_{S-S} with molecular length $N_C = 10$.

the heat current and the temperature difference (c) and (d), where again one needs to remember that the heat current is fixed in simulations and the temperature difference is the calculated-simulated value. Appendix A provides details of the setup and the simulation procedure. The force field and its parameters are described in Appendix C.

Focusing on Fig. 1(b), which exemplifies the characteristics of the temperature profile, we point out that its form agrees with the literature. 15,24 Note the large temperature fluctuations on the S and C atoms, compared with the Au sections. This is expected since each gold section consists of many (270) atoms, allowing better averaging and reduced fluctuations within the leads—compared with molecular sections, which are made of single atoms. Additional observations are the following: (i) A small gradient is presented within the Au sections. (ii) The temperature profile is approximately spatially symmetric, reflecting the structural symmetry. (iii) The lion's share of the temperature bias drops at the interfaces between the gold leads and the sulfur atoms. Only a small temperature gradient develops on the alkane chain itself. This behavior matches the fact that the harmonic part of the molecular force field dominates over anharmonic contributions, thus transport on the molecule is close to ballistic⁴² (anharmonic interactions are included in the molecular dihedral and Au-interface interactions). Metal-molecule interfacial thermal resistance⁴³ is, thus the main source of resistance in Au-alkanedithiol-Au junctions, as we also show in Fig. 2.

The results in Figs. 1(c) and 1(d) demonstrate a linear relationship between the heat current and the temperature difference, allowing us to extract both G_{Au-Au} and G_{S-S} as linear response coefficients. The molecule-length dependency of both G_{Au-Au} and G_{S-S}

is shown in Fig. 2. While G appears to be higher at short lengths, the thermal conductance is approximately constant for chains with $N_{\rm C}=8-12$ units, yet manifesting a small decline for longer chains. Based on the dominance of the harmonic part in the alkane

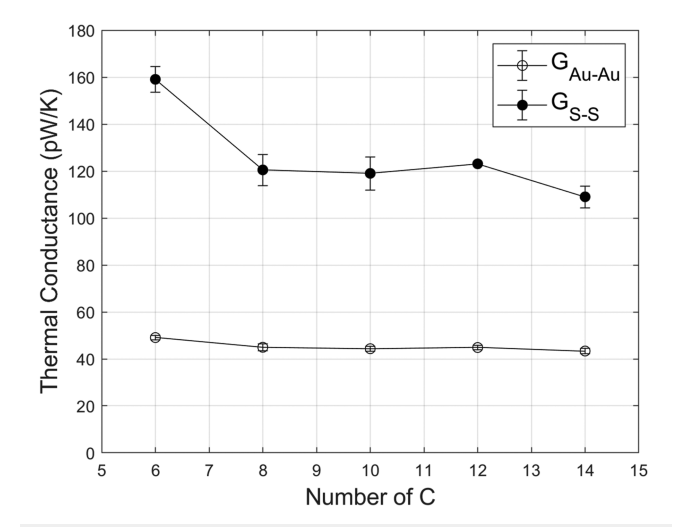


FIG. 2. RNEMD thermal conductance as a function of molecular length displaying $G_{\text{Au-Au}}$ and $G_{\text{S-S}}$. Data were obtained by performing simulations as presented in Fig. 1 while varying the molecular length: For each junction, the heat current is set at J=0.02 eV/ps, and we extract the temperature differences $\Delta T_{\text{Au-Au}}$ and $\Delta T_{\text{S-S}}$ to evaluate the respective conductance. Each data point was averaged over three independent simulations.

force-field, alkane-based junctions are expected to follow the ballistic transport behavior, with minimal inelastic-dissipative effects. The ballistic mechanism in our system is reflected by the thermal conductance being almost independent with length, and it is supported by experiment. However, other studies of alkane chains discovered that finite-size effects can cause the thermal conductance to peak at short molecular lengths. 10,23

Our calculated Au-to-Au thermal conductance, $G_{\rm Au-Au}$, is in a good agreement with the literature, both in terms of values and trends, see Sec. II C. In what follows: unless otherwise stated, we use $G_{\rm M-M'}$ as the relevant measure for the junction's conductance, with the temperature difference evaluated from the metal atoms at the boundaries.

Examining in Fig. 2 the intrinsic conductance, G_{S-S} , we observe similar trends to G_{Au-Au} , with the conductance close to saturating for long chains. As expected, the intrinsic molecular conductance is greater than the junction's value, $G_{S-S} > G_{Au-Au}$, reflecting the contribution of contact resistance to the latter. It is remarkable to note the extent of the suppression of conductance due to the interface

resistance. This reinforces the argument that transport is close to being ballistic (nonresistive) in the molecule.⁶

B. Approach-to-equilibrium molecular dynamics

The AEMD method relies on the phenomenological Newton's law of cooling. In this method, the thermal conductance is determined from the rate of thermal equilibration of the metal leads. Starting with a nonequilibrium condition, the two separate metal leads are prepared at distinct temperatures, hot and cold. Once the metals are attached via the molecule, energy flows between the metals through the molecule, approaching a global equilibrium state. By monitoring the bulk temperature while relaxing to equilibrium, one can determine the thermal conductance of the junction.

Newton's cooling law for each metal lead is given by

$$C\frac{dT_h(t)}{dt} = -G[T_h(t) - T_c(t)],$$

$$C\frac{dT_c(t)}{dt} = -G[T_c(t) - T_h(t)],$$
(2)

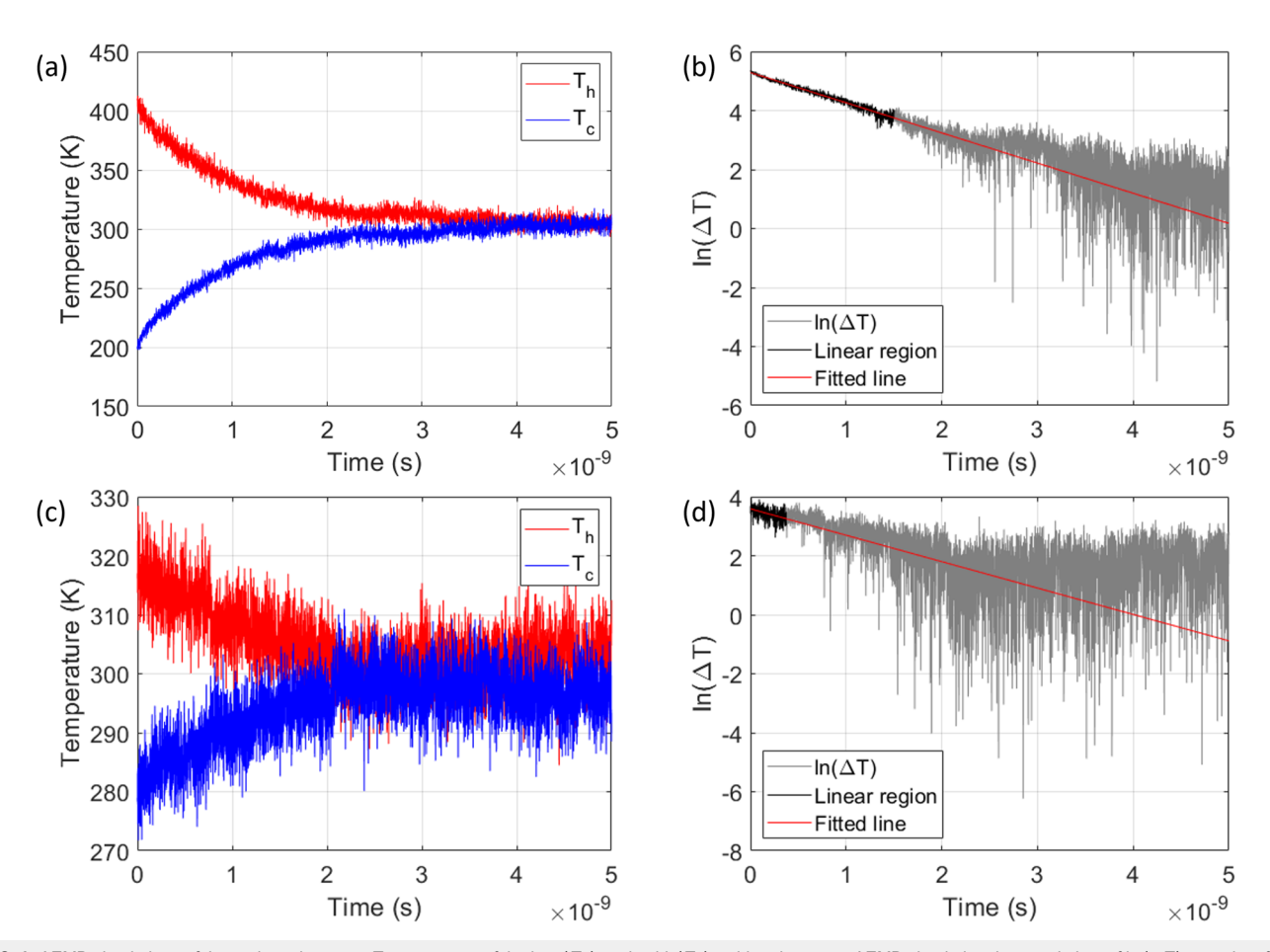


FIG. 3. AEMD simulations of thermal conductance. Temperatures of the hot (T_h) and cold (T_c) gold regions over AEMD simulation time, and plots of $\ln(\Delta T)$ over time for (a) and (b) initial temperature bias of 200 K and (c) and (d) 50 K. The decay timescale τ used in the determination of the thermal conductance, Eq. (5), is obtained from a linear fit of the $\ln(\Delta T)$ plot before equilibration. Panels (c) and (d) highlight the limitation of the AEMD method at low temperature biases, as the exponential decay toward equilibrium is not sufficiently manifested. Parameters are $N_C = 10$ in both cases and $\bar{T}(0) = 300$ K.

where C is the heat capacity of the lead. Using the Dulong–Petit law, which is justified in the classical MD simulations, the heat capacity is approximated as $C = 3k_BN_{\rm Au}$, where N is the number of moving gold atoms in the lead (see Appendixes A and B) atoms, and k_B is the Boltzmann constant. G is the thermal conductance of the junction. Defining the temperature difference as $\Delta T = T_h - T_c$, the two parts of Eq. (2) can be combined,

$$\frac{d\Delta T(t)}{dt} = -\frac{2G}{C}\Delta T(t). \tag{3}$$

The solution to this differential equation is given by

$$\Delta T(t) = \Delta T(0) e^{-t/\tau}, \tag{4}$$

where $\tau \equiv C/2G$ is the equilibration time. For later use, we also define the averaged temperature as $\bar{T}(t) = [T_h(t) + T_c(t)]/2$, which is set at $\bar{T}(0) = 300$ K for the AEMD simulations.

We display examples of AEMD simulations in Fig. 3 with initial temperature biases of 200 K (top) and 50 K (bottom). Raw data with the changing temperatures of the metals is shown in Figs. 3(a) and 3(c). In Figs. 3(b) and 3(d), we present $\ln(\Delta T)$ as a function of time in accord with Eq. (4). While at short times an exponential decay is observed (linear decay in the log scale), at long time the system approaches equilibrium and it no longer follows Newton's cooling law. Focusing on the appropriate exponential-decay regime, colored in black in Figs. 3(b) and 3(d), one can extract the slope $1/\tau$ and evaluate the thermal conductance from the AEMD method as

$$G = \frac{C}{2\tau}. (5)$$

In Fig. 4, we show that thermal conductances from the AEMD method are in agreement with RNEMD results for $G_{\text{Au-Au}}$. While larger errors seem to affect the conductance in AEMD, results are

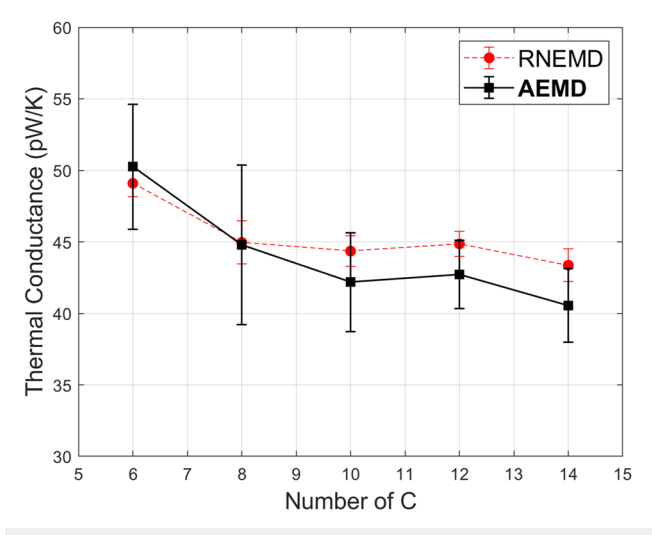


FIG. 4. AEMD simulations of thermal conductance as a function of molecular length (\square). RNEMD results from Fig. 2(a) are overlayed for comparison (\circ). Parameters are $T_h(0)=400$ K, $T_c(0)=200$ K. Each AEMD data point was obtained by averaging over five runs.

within repeated simulation error, and trends observed in the two methods are similar. The AEMD method thus similarly exposes an approximate ballistic transport behavior, compounded with finite-size effects. ¹⁰

While Fig. 4 suggests that RNEMD and the AEMD are both valid, there are several limiting aspects of the AEMD method that make it less favorable than RNEMD. These aspects are discussed in Sec. II C, concluding that the RNEMD method is a more robust technique. Thus, our method of choice in applications, Sec. III, is RNEMD.

C. Comparison: Methods and experiments

The results from the RNEMD and AEMD methods match well, as we show in Fig. 4. While both methods display what seems to be finite-size effects of the conductance in short chains, ballistic transport is more evident in RNEMD results for longer systems.

We now discuss the pros and cons of the two methods. Beginning with the RNEMD method, the determination of thermal conductance in this technique is based on measuring the temperature profile along the chain, in a steady state. This method, however, is not limited to linear-response, as one can more generally interrogate with RNEMD the relationship between ΔT and the heat current, as we do in Sec. III. On the down side, production runs with RNEMD are relatively long, at ≈ 25 ns, an order of magnitude longer than AEMD simulations [see Figs. 3(a) and 3(c)]. Indeed, the main appealing aspect of the AEMD is its shorter simulation time with decreased computational cost.

Despite its short simulation time, the AEMD method suffers from several deficiencies. Newton's cooling law is phenomenological and it relies on several assumptions including that *G* is temperatureindependent and that the decay behavior is controlled by a single timescale. Regarding the former, this issue will be of a concern in systems for which G varies with temperature with problems expected to be manifested when going to high temperature biases. A second limitation of AEMD concerns studies at small biases. As noted in Fig. 4, simulations of *G* over length were obtained using a temperature bias of 200 K, which is larger than what experiments nowadays can feasibly allow. 18,19 Thus, we attempted to determine G with AEMD at a lower bias, comparable to the aforementioned experiments. Raw data are displayed in Figs. 3(c) and 3(d). We immediately note the extent of fluctuations in the temperature trajectory due to the small temperature bias in Fig. 3(c), compared with Fig. 3(a). These fluctuations, and the short equilibration time limit the adoption of the AEMD cooling equations. Figure 3(d) shows that the linear region is short and noisy, thus extracting the timescale τ is imprecise. Indeed, our fitting procedure leads to a G value of 35 pW/K, which is outside the range of results in Fig. 4. Additional constraints on the AEMD method are that it assumes that there is no spatial variation of the temperature in the bulk, and that it is not proper to be used on long molecular systems because the phenomenological cooling expression assumes a single exponential decay. In contrast, in long chains (N = 14 according to our tests) oscillations decorate the exponential decay, indicating more involved dynamics than a single exponential

Based on both RNEMD and AEMD methods, the thermal conductance of single-molecule S-alkane-S junction of $N_{\rm C}\approx 10$ sites is at 40–45 pW/K. In Table I, we compile relevant thermal conductance values from the literature for alkane junctions, both

TABLE I. Table of thermal conductance values from theoretical and experimental studies.^a

Nos.	Reported conductance	Molecule type	Interface type	Single-molecule/SAM	Experiment/theory	Authors
1	40-45 pW/K	S-alkane-S	Au	Single-molecule	Theory (classical MD)	This work
2	30 pW/K	Alkane	Debye-type model	Single-molecule	Theory (GQLE)	Segal et al. ¹⁰
3	20 pW/K	S-alkane-S	Au	Single-molecule	Theory (classical MD)	Sharony <i>et al.</i> ¹⁵
4	39 pW/K	S-alkane-S	Au	Single-molecule	Theory (classical MD)	Majumdar <i>et al</i> . ²⁵
5	30-35 pW/K	S-alkane-S	Au	Single-molecule	Theory (semiclassical MD)	Li <i>et al</i> . 16
6	35-45 pW/K	S-alkane-S	Au	Single-molecule	Theory (quantum NEGF)	Klöckner et al. ¹²
7	180 pW/K	Alkane	Si	Single-molecule	Theory (classical MD)	Sasikumar and Keblinski ¹¹
8	25 pW/K	S-alkane-S	Au	Single-molecule	Experiment	Cui et al. ¹⁸
9	40 pW/K	S-alkane-S	Au	Single-molecule	Experiment	Mosso et al. ¹⁹
10	$400 \text{ MW/m}^2 \text{ K}$	S-alkane-S	Au	SAM	Theory (classical MD)	Luo and Lloyd ²⁶
11	$260 \text{ MW/m}^2 \text{ K}$	Alkane	Si	SAM	Theory (first-principles AEMD)	Duong et al. ³³
12	$18 \text{ MW/m}^2 \text{ K}$	Alkane	Diamond	SAM	Theory (classical MD)	Wang et al. ²⁹
13	$60 \text{ MW/m}^2 \text{ K}$	S-alkane-S	Au	SAM	Experiment	Majumdar <i>et al.</i> ²⁴
14	16 pW/K	S-alkane	Au, Si	SAM	Experiment	Meier <i>et al.</i> ²³

^aReported G are those most relevant to our system, such as the approximate thermal conductance of a ten-carbon chain, if the authors examined length dependence.

computational with different methods, as well as experimental; our obtained results (row No. 1) should be compared with relevant experimental studies (row Nos. 8 and 9), as well as to computations on the same system (row Nos. 3–6). SAMs bring comparable values when consideration is given to the per area aspect of their thermal conductance.

In Ref. 10 (row No. 2 in Table I), Generalized Quantum Langevin Equation (GQLE) simulations were used to estimate the thermal conductance of alkane chains connected to solids, resulting in conductances of ~ 30 pW/K at room temperature for a ten-atom alkane chain. While this number is surprisingly close to experimental results, we note that in the GQLE the interface is lacking chemical information: The solids are described in a stochastic manner and one uses a simple analytic form for their density of states.

III. THERMAL DIODE EFFECT

The development of molecule-based thermal devices is a central objective in nanoscale heat transport, with a particular interest in the realization of thermal diodes (rectifiers).^{2,9} In analogy to electrical diodes, thermal diodes present differences in the magnitude of the heat current when the direction of the applied temperature bias is reversed. Early studies identified anharmonicity and spatial asymmetry as two key factors in realizing thermal diodes, and efforts were placed on identifying promising molecular and nanoscale setups. 36-40 More recently, advancements in studies of phononic thermal diodes have largely occurred through MD simulations of carbon-based materials. 44-49 In parallel to the quest for realizing molecular-based heat diodes, radiative thermal diodes were explored in hybrid normal-superconducting junctions^{50–52} and by utilizing metal-insulator phase transitions;⁵³⁻⁵⁵ these references are examples of a large literature. Additionally, pump-probe time-dependent studies on asymmetric molecules discovered unidirectional vibrational energy flow, a diode-like effect. 56-58 Overall, compared with the electrical analog, thermal control is hindered by immature technology; studies of thermal diodes may lead to the development of desired nonlinear thermal components.

Our objective in this section is to test whether alkane junctions, which were already studied as thermal conductors, can be modified and used as backbone materials in phononic thermal diodes. Recalling that anharmonicity and spatial asymmetry are necessary conditions in the thermal diode effect, we note that anharmonicity is built-in into the alkanedithiol junction in several places: within dihedral interactions, the Morse potential at the boundary in the Au–S bond, and the contribution of the Lennard-Jones and embedded atom model (EAM) potentials. As for structural asymmetry, we introduce it here either by modifying one of the endgroups, or by replacing one of the metal leads. In both setups, the thermal transport behavior is examined with the RNEMD method, which allows the investigation of current-temperature bias characteristics far from equilibrium.

In Sec. II, we showed that the thermal conductance of alkanedithiol junctions was about a constant, independent of length. This suggests ballistic transport as the ruling transport mechanism, resulting from the dominance of harmonic interactions over anharmonic effects. Note that in Fig. 2 the temperature difference $\Delta T_{\text{Au-Au}}$ was at about 60 K. However, a diode effect is a nonlinear transport phenomenon that shows up at a high bias, once nonlinear contributions in ΔT manifest, $J \approx G\Delta T + G_2(\Delta T)^2 + \cdots$. Here, G is the (linear response) thermal conductance, and G_2 is the first nonlinear contribution to the diode effect. While the linear-response conductance may predominantly reflect the harmonic force field, even-power terms such as G2 fundamentally rely on anharmonic interactions. To realize a thermal diode, we thus need to amplify anharmonic effects in the junction, enhance spatial asymmetry, and most importantly, apply a large thermal bias so as to increase the weight of high-order terms in the current, such as $G_2(\Delta T)^2$. Below, we apply large thermal biases as high as $\Delta T = 500$ K.

A. Asymmetric endgroups and the thermal diode effect

Our first proposed setup for single-molecule thermal diodes is depicted in Fig. 5. It includes an alkane chain with endgroups

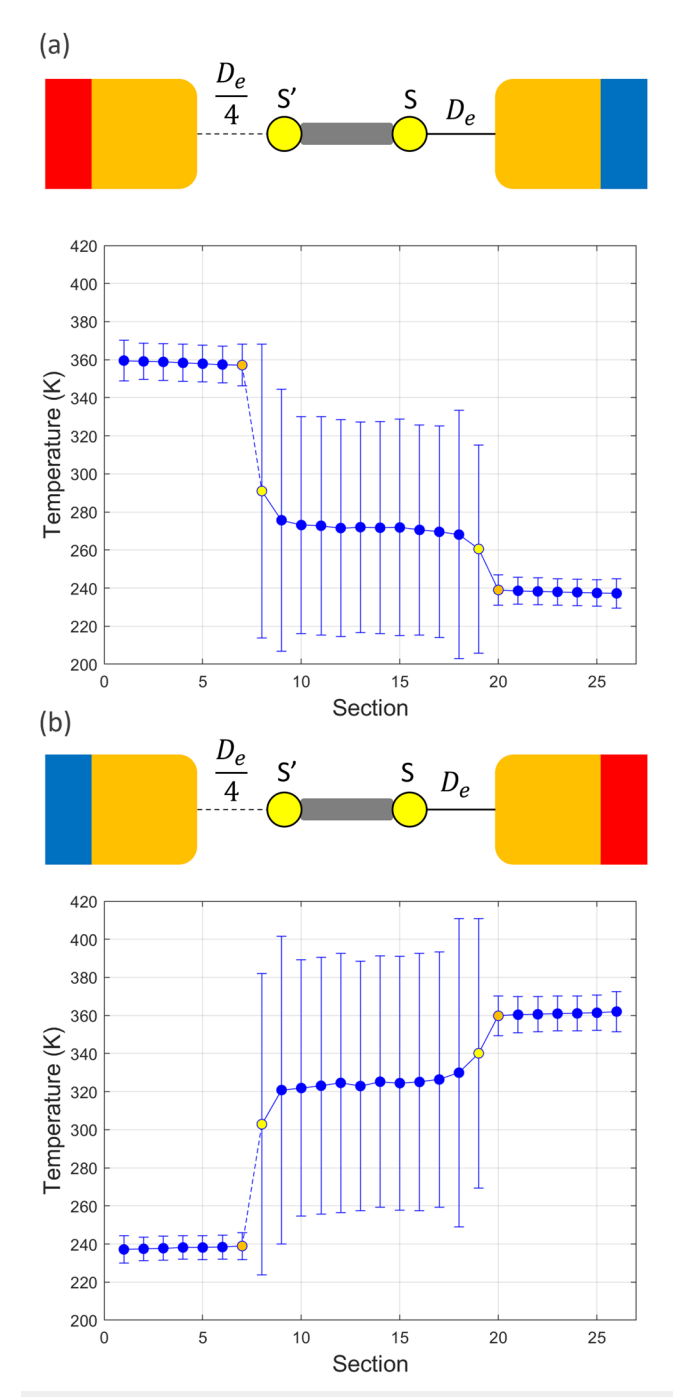


FIG. 5. Asymmetric junctions created by manipulating the dissociation energy of endgroups connected to Au. (a) and (b) show two identical, asymmetric junctions with imposed heat current flowing in opposite directions. The respective temperature profiles from RNEMD are displayed, manifesting a large jump in temperature at the weaker contact. Parameters are heat current of $J=0.02\,\mathrm{eV/ps}$ and $N_{\mathrm{C}}=10$.

of distinct bond dissociation energies. Specifically, we assume that one endgroup involves a "normal" Au-S bond, while the potential energy of the opposite endgroup denoted by S' is weakened using a smaller bond dissociation energy, $D_e/4$. We refer to the Au-S

and $\operatorname{Au-S'}$ contacts as "strong" and "weak," respectively. Specifically, the D_e values in the Morse potential are 0.38 eV (strong) and 0.095 eV (weak). As such, we created an asymmetric junction as well as enhanced the role of anharmonicity. The weaker endgroup could represent an Au-methyl or Au-carboxilic contact. Since our goal here is to explore different setups toward thermal diode applications, we rely here on this phenomenological and flexible mean for enforcing asymmetry, rather than analyze a concrete endgroup.

For comparison, we first study a symmetric junction where both contacts are weak, and find (simulation results not shown) that the thermal conductances $G_{\text{Au-Au}}$ and $G_{\text{S-S}}$ are in the range of 20–22 and 96–105 pW/K, respectively. Thus, with weak bonds, the junction's conductance $G_{\text{Au-Au}}$ is approximately half of the value obtained with normal S-bond interactions (see Fig. 2). In contrast, and in accord with our expectations, the *molecular* conductance of weakly bonded junctions is only mildly (~15%) smaller than the strongly bonded junction's value.

We exemplify in Fig. 5 the temperature profile generated in a current-carrying nonequilibrium situation under forward and reversed currents of the same magnitude. A large temperature drop occurs on the weakly-coupled contact S'-Au, while a smaller temperature difference falls on the stronger S-Au contact. This is expected; the stronger bond better facilitates thermal transport with reduced contact resistance. The temperature of the alkane chain thus lies closer to the temperature of the Au lead to which it strongly couples.

In Fig. 5, we enforced identical currents in opposite directions. However, to test the existence and extent of the diode effect one needs to compare $J(\Delta T)$ to $J(-\Delta T)$. This is a nontrivial task under the RNEMD method since in this approach we impose currents and gain the corresponding ΔT as the dependent variable.

Figure 6(a) illustrates the diode setup. Results are presented in Figs. 6(b) and 6(c) showing the heat currents for the asymmetric D_e junctions as a function of the junction's thermal bias, $\Delta T_{\rm Au-Au}$, and as a function of the intrinsic bias, $\Delta T_{\rm S-S'}$. Recall that the latter bias corresponds to the temperature difference falling on the molecule, between the two endgroups.

When the system operates as a diode, the current-bias profiles of forward and backward junctions should differ, $|J(\Delta T)|$ $\neq |J(-\Delta T)|$. To guide the eye, we project the forward current onto the left-bottom quadrature. Figure 6(b) displays this plot against $\Delta T_{\text{Au-Au}}$, and we find that the diode effect on the junction is marginal. Thus, though (as we show next) a small diode effect exists on the molecule, transport asymmetry is negligible once taking into account the contribution of contact resistance. Given the approximate linear current-bias trend, we can also extract the conductance, which is ~27 pW/K. In Fig. 6(c) we present the current against the *internal* temperature drop, $\Delta T_{S-S'}$. In this case, we do observe a small diode effect: The comparison between current-bias profiles indicates that the current is larger when the weak bond is coupled to the hot metal, than when the weak bond is connected to the cold bath, in accord with Refs. 39 and 40. Nevertheless, (i) a diode effect is missing in the junction's definition. (ii) Even when utilizing the intrinsic definition, the diode effect is small. We thus conclude that a diode effect is marginal in asymmetric-endgroup alkane junctions under experimentally relevant applied biases.

B. Mismatched metals and the diode effect

We explore here the development of the diode effect in asymmetric junctions created by replacing one of the gold contacts with

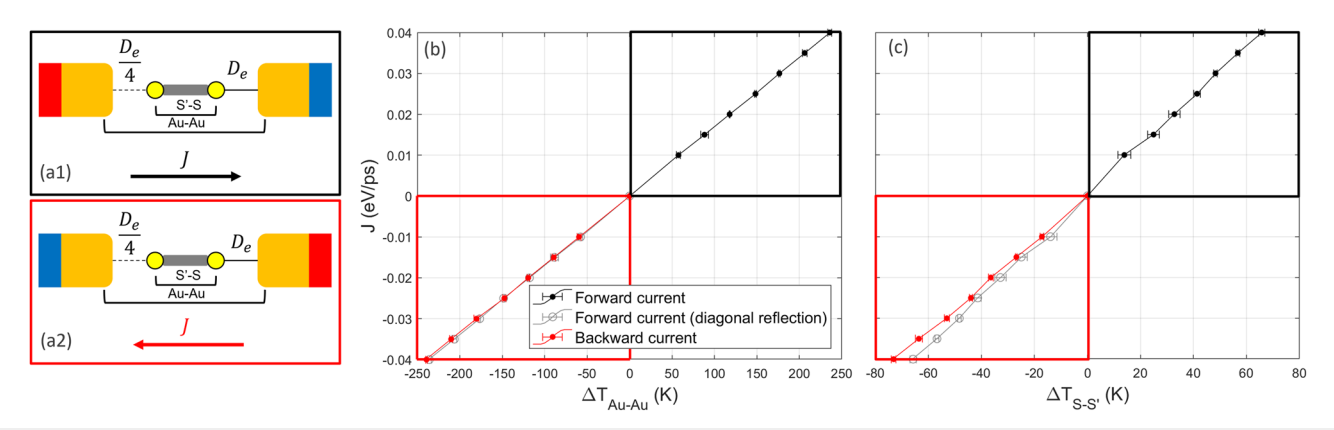


FIG. 6. Analysis of the thermal diode effect in junctions with endgroup asymmetry. (a1) and (a2) Graphical representation of molecular junctions in the (a1) forward and (a2) backward current direction. (b) and (c) Imposed forward (black) and backward (red) currents against (b) $\Delta T_{\text{Au-Au}}$ and (c) $\Delta T_{\text{S-S'}}$. The forward current is also diagonally projected on the left-bottom quadrature (gray, empty \circ). In simulations, $N_{\text{C}} = 10$, the heat current was varied, and the temperature bias was extracted as explained in Fig. 5.

a different metal, silver. Silver has a higher Debye temperature than gold, $T_D^{\rm Au}=180$ K, while $T_D^{\rm Ag}=220$ K. In Au-SAM-Ag junctions, the mismatch in phononic spectral densities of the different metals was shown experimentally to impact (reduce) thermal transport compared with an Au-SAM-Au junction. ²⁴ It is interesting to probe this effect in single-molecule junctions, as well as to test whether it could lead to a diode effect under large temperature biases.

In simulations, we replaced one of the gold contacts by silver, changing the atomic mass and the metal–metal interaction (EAM potential). However, we assumed that Au and Ag have identical Morse interaction potentials with the molecular endgroup (S). This assumption allows us to concentrate on the role of the mismatch in the phonon spectra of the metals on the diode effect, rather than compounding it with the impact of different endgroups' interactions.

We display in Fig. 7 a graphical representation of a junction with mismatched metals, along with the temperature profiles under forward and backward current-carrying conditions. Similar to Fig. 5, we observe that the averaged temperatures of the backbone C atoms deviate from $T \approx 300~\rm K$ (the temperature achieved in symmetric junctions, see Fig. 1). Instead, the temperature of the molecule lies closer to the temperature of Ag. Comparison with Sec. III A suggests that Ag, with its higher Debye frequency, allows better phonon transmission to the molecule, thus a smaller contact resistance. As for the internal temperature profile, we find that it is symmetric under the reversal of the nonequilibrium condition.

We now probe the diode effect in junctions with mismatched metals and compare it to the case with asymmetric endgroups. The results are presented in Fig. 8. For small currents, we confirm a linear trend with $J(+\Delta T) = -J(-\Delta T)$. When we test the behavior under high heat currents, $\Delta T_{\rm M-M'}$ begins to differ when evaluated in the forward or backward directions, with significant deviations once $\Delta T_{\rm M-M'} > 200$ K. A clear diode effect shows once the metals are maintained at large temperature differences of 300 K and higher. Note that for J = 0.1 eV/ps, we found that the temperatures of the hot and cold metals were ~450 and 150 K, which can be still simulated with classical MD.¹⁶ In contrast, for J = 0.15 eV/ps,

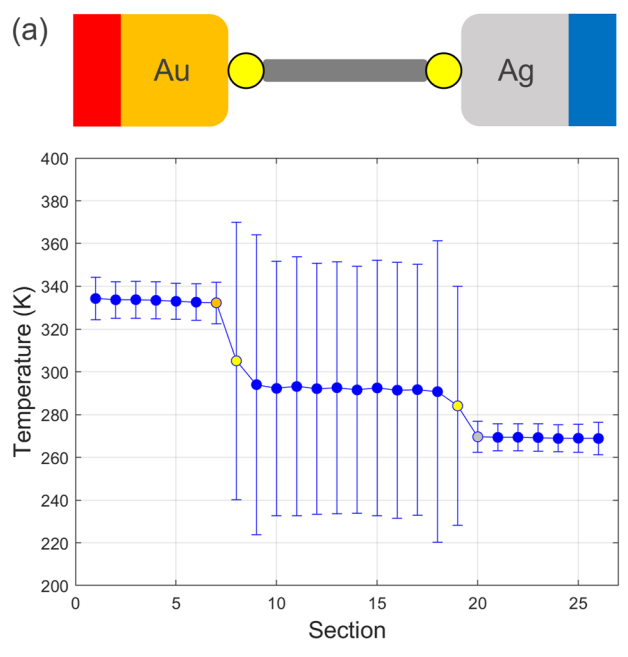
the corresponding temperatures were about 550 and 50 K; for this, low temperature classical simulations lose accuracy. ¹⁶ Nevertheless, as we mention below, building $\Delta T \sim 500$ K over 1–2 nm junctions is not feasible. As for the internal temperature difference, $\Delta T_{\rm S-S}$, we also observe a substantial diode effect forming internally, and at lower temperature biases than when measured at the contacts, although simulation noise clouds this observation. These results are in line with the behavior of the asymmetric-endgroup junctions as presented in Fig. 6, where the internal molecular definition manifested a more noticeable diode effect compared with the marginal metal-to-metal result.

Overall, according to Fig. 8, mismatched junctions do not support a substantial diode effect as long as $\Delta T_{\rm M-M'} < 200$ K. While the mismatched metals can support a diode effect, the temperature difference required for its manifestation is outside of what is feasible in experiments, which typically stays in the range of $\Delta T = 50$ –100 K.

Asymmetry was introduced here in the metals' phonon spectra. We recall a related setup, which does not involve metal contacts: Motivated by pump-probe experiments in solution, ^{56,57} in Ref. 59 a diode-like effect was analyzed in a molecules consisting two distinct endgroup moieties, anthracene and azulene, bridged by a polyethylene glycol oligomer. There, a significant diode effect was observed on the molecule due to the vibrational mismatch between the two endgroups, combined with nonlinear-anharmonic coupling effects.

C. Discussion

The junctions analyzed in Secs. III A and III B were spatially asymmetric, and they involved anharmonic effects. However, only at challenging conditions of high thermal biases could a diode effect be realized. We recall that in Sec. II, we observed that the thermal conductance of the junctions only weakly varied with size, indicating the dominance of the harmonic force field in thermal energy transport. Here, pushing the mismatched case to high thermal biases, we expose the G_2 term [recall the series expansion $J \approx G\Delta T + G_2(\Delta T)^2 + \cdots$]. This term, and higher even-power terms are responsible for the diode effect.



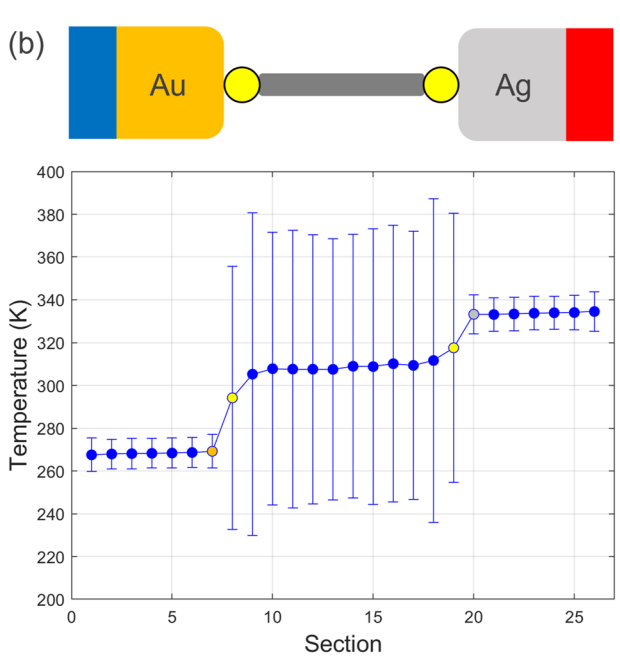


FIG. 7. Thermal transport in Au-alkanedithiol-Ag junctions. (a) and (b) show two identical junctions with heat currents flowing in opposite directions, along with their respective temperature profiles (RNEMD simulations). Parameters are heat current J=0.02 eV/ps and $N_{\rm C}=10$.

We estimate the nonlinear contribution G_2 in our system using data from Fig. 8. Consider say the case of J = 0.15 eV/ps: In what we refer to as the forward (F) direction, the M-M' temperature drop is $\Delta T_F = 465$ K while in the opposite, backward (B) scenario

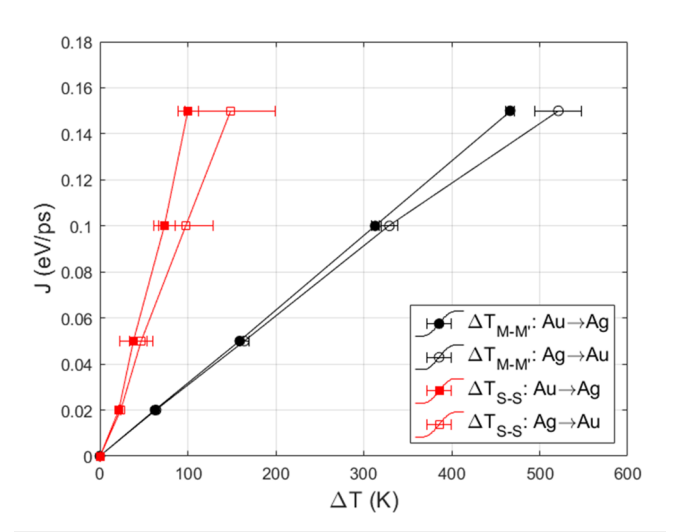


FIG. 8. Study of a diode effect in Au-alkanedithiol-Ag junctions, extending to large heat current and temperature differences. We present the current from the hot Au to the colder Ag (full) and the reversed configuration (empty) as a function of the temperature bias between the metals (circle) or the endgroups (square). The temperature differences $\Delta T_{\text{S-S}}$ and $\Delta T_{\text{M-M'}}$ were calculated based on profiles as in Fig. 7. Simulations were performed with the RNEMD method on an $N_{\text{C}}=10$ chain

 $\Delta T_B = 520$ K. Using the polynomial expansion for the current, we find that

$$G_2 = G \frac{\left(\Delta T_B - \Delta T_F\right)}{\Delta T_F^2 + \Delta T_R^2}.$$
 (6)

Plugging the above values for the temperature differences and using the linear conductance $G = 3.2 \times 10^{-4}$ eV/(ps K) (equivalent to about 50 pW/K), we estimate $G_2 = 3.6 \times 10^{-8}$ eV/(ps K²), which is 0.006 pW/K². Clearly, our system requires large thermal biases to manifest the impact of G_2 .

The absence of the diode effect under moderate conditions could be analyzed as follows:⁶⁰

In both setups (junctions with distinct endgroups or mismatched metals) and under moderate currents of J = 0.02 eV/ps (which is not far from what was used in experiments such as in Ref. 18, at about 0.0075 eV/ps), the temperature profile approximately obeys the following relation,

$$T_n + \tilde{T}_n = T_M + T_{M'} = 2\bar{T}.$$
 (7)

Here, T_n is the temperature of the nth section (part of the metal, or of the molecule) under left-to-right net current, while \tilde{T}_n is the temperature profile under reversed conditions. $T_{\mathrm{M,M'}}$ are the temperatures of the metals measured at their boundaries, with \bar{T} defined as their average.

We now assume that the heat current can be written as a linear function in the local temperatures,

$$J_{\mathrm{M}\to\mathrm{M}'} = \sum_{n} \alpha_n T_n,\tag{8}$$

with α_n as the expansion coefficients. Based on the fact that J=0 at equilibrium, we find that $\sum_n \alpha_n = 0$. Now, to test the diode effect, we turn the bias such that now heat flows from M' toward M. We thus use the temperature profile of the reversed case,

$$J_{M' \to M} = \sum_{n} \alpha_{n} \tilde{T}_{n},$$

$$= \sum_{n} \alpha_{n} (T_{M} + T_{M'} - T_{n})$$

$$= -\sum_{n} \alpha_{n} T_{n},$$
(9)

which proves the absence of a diode effect. Note that Eq. (8) extends beyond a Landauer-harmonic description and it could account for anharmonic effects and high thermal biases situations, see, e.g., Ref. 60. Thus, as long as (i) the temperature profile obeys the symmetry relation Eq. (7), and the current is linear in the local temperatures, Eq. (8), a diode effect cannot be materialized in the junction. Figures 5 and 6 for asymmetric endgroups, and Fig. 7 with Fig. 8 for mismatched metals, support this analysis.

IV. MISMATCHED JUNCTIONS: SINGLE-MOLECULE VS SELF-ASSEMBLED MONOLAYERS

We now go back to the linear-response regime and address a question that was previously interrogated for SAMs in Ref. 24: What is the role of mismatched metals on the junction's linear response thermal conductance? We return to the conditions of Fig. 7 where the current was relatively low, yielding $\Delta T_{\rm M-M'}\approx 60$ K. In this regime, the heat current vs $\Delta T_{\rm M-M'}$ trend is about linear, thus one can calculate the linear conductance on the junction from their ratio. We present in Fig. 9 the thermal conductance of this system, testing junctions with the same metals (Au-alkane-Au and Ag-Alkane-Ag), and with mismatched interfaces (Au-alkane-Ag and Ag-alkane-Au).

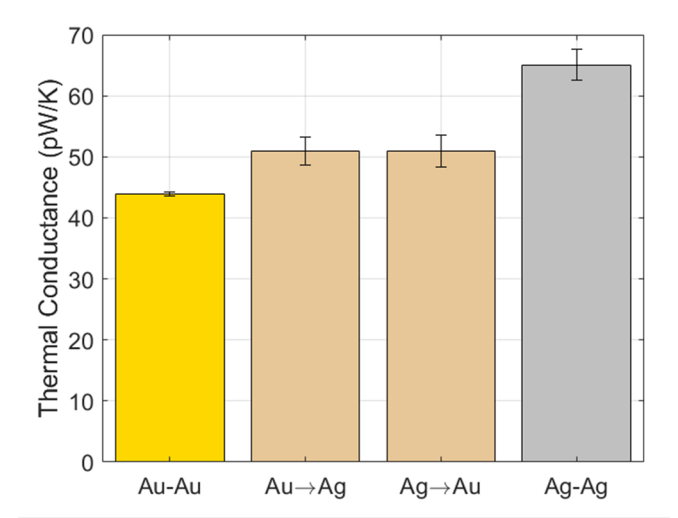


FIG. 9. Thermal conductance in M-alkanedithiol-M $^\prime$ junctions with Au and Ag metals. The arrow in the labeling of asymmetric junctions indicates the direction of net heat flow, from the hot to the cold metal. Parameters are heat current J=0.02 eV/ps and $N_{\rm C}=10$.

We reveal that the conductance with Ag metals is *higher* than with Au. As for the mismatched junctions, they support conductances in between those of the homogeneous-metal junctions.

A previous RNEMD study on SAMs compared the conductance of Au-alkanedithiol-Au to Au-alkanedithiol-Ag,²⁴ observing a higher thermal conductance in the latter system. Experiments on SAMs,²⁴ however, showed the opposite trend, with mismatched junctions having conductance below the homogeneous-gold case. This disagreement was suggested to stem from classical MD simulations activating high-frequency vibrational modes, which in actuality should not participate in heat transport. A simple harmonic theory for heat transport is presented in Appendix D. This harmonic analysis supports MD predictions with the ordering $G_{Ag-Ag} > G_{Au-Au}$. However, under the harmonic approximation of Appendix D, the mismatched junction conducts similar to the homogeneous gold case. These points to the fact that the impact of anharmonic interactions can be discerned from analysis of mismatched junctions, and that these interactions are apparently at play in our molecular junctions.

V. SUMMARY

Using classical molecular dynamics simulations, we studied phonon heat transport through single molecule junctions. The work addressed two aspects: Method development in the area of classical molecular dynamics, and applications, interrogating whether alkane-based molecular junctions could be modified to serve as thermal diodes.

In the method-development part of this study, we employed two classical MD methods. RNEMD is a steady-state approach where one sets the current and obtains the temperature profile across the junction, allowing the calculation of current-bias characteristics and the thermal conductance. In contrast, in the AEMD method, one follows the equilibration dynamics from a nonequilibrium initial condition, receiving the junction's conductance, albeit under some approximations.

The two methods produced similar results for the thermal conductance of 6 to 14-unit Au-alkanedithiol-Au junctions. Results were in accord with reported experiments, pointing as well to the expected ballistic transport. Though the AEMD method offers a computational advantage over the RNEMD technique, we concluded that assumptions underlying its analysis restrict its application (e.g., to large thermal biases ΔT) deeming the RNEMD method to be a more suitable, flexible, and robust method to study thermal transport in molecular junctions.

By constructing spatially asymmetric junctions, we probed the diode effect in alkane-based junctions far from equilibrium. We constructed two setups: molecules with asymmetric endgroups of strong and weak bonds, and molecules placed between different (mismatched) metals. In both cases, the temperature profile generated on the current-carrying junction was spatially asymmetric. In junctions with asymmetric endgroups, a large temperature gradient developed on the weak contact, yet the diode effect when measured on the junction (rather than over the molecule) was marginal. For Au-alkane-Ag mismatched junctions, the Au contact was more resistive, with a larger thermal bias falling on that contact. In the mismatched case, we had pushed the thermal bias to significantly high values and then showed that a diode effect could be materialized. We

thus conclude that alkane-based junctions with mismatched metals show a thermal diode effect once large thermal biases (over 300 K) are applied. These conditions are beyond current experimental capabilities.

Moving beyond alkane-based chains, which serve here as a benchmark, our future work will be focused on the simulation of phonon heat transport in families of flexible molecules that are expected to show nonlinear transport behavior at moderate thermal biases, thus possibly support a stronger diode response. In addition, there is an interest in identifying families of molecules that either promote⁶¹ or hinder^{62,63} thermal transport in single-molecule junctions.

Other fundamental challenges in molecular thermal transport include (i) performing a quantitative study of the relationship between transient pump-probe vibrational energy transfer experiments 64-66 and steady state measurements of phononic heat transport; (ii) identifying means for an active control of thermal transport, e.g., with electric fields⁶⁷ or by mechanical compression;68 and (iii) understanding whether and when quantum effects contribute to steady-state phonon transport at room temperature. 5,16,69

ACKNOWLEDGMENTS

D.S. acknowledges the NSERC discovery grant and the Canada Research Chair Program. A.J.H.M. acknowledges National Science Foundation Award No. DMR-2025013.

AUTHOR DECLARATIONS

Conflict of Interest

The authors have no conflicts to disclose.

Author Contributions

Jonathan J. Wang: Conceptualization (equal); Data curation (lead); Formal analysis (lead); Investigation (lead); Methodology (equal); Software (lead); Validation (equal); Visualization (lead); Writing original draft (lead); Writing - review & editing (equal). Jie Gong: Formal analysis (equal); Investigation (equal); Methodology (supporting); Software (supporting); Supervision (supporting); Validation (equal); Writing - original draft (supporting); Writing review & editing (equal). Alan J. H. McGaughey: Formal analysis (equal); Investigation (equal); Methodology (equal); Project administration (supporting); Software (supporting); Supervision (supporting); Validation (equal); Writing - original draft (supporting); Writing - review & editing (equal). Dvira Segal: Conceptualization (lead); Data curation (equal); Formal analysis (equal); Funding acquisition (equal); Investigation (equal); Methodology (equal); Project administration (lead); Supervision (lead); Validation (equal); Visualization (equal); Writing - original draft (equal); Writing review & editing (equal).

DATA AVAILABILITY

The data that support the findings of this study are available from the corresponding author upon reasonable request.

APPENDIX A: IMPLEMENTATION OF RNEMD SIMULATIONS

We describe here technical details concerning the RNEMD method. We present the setup and simulations for the junction. One can readily generalize the setups to account for a modified sulfur endgroup, S', and use other metal contacts.

1. Setup

The initial, rigid structure of the system is displayed in Fig. 10, where a single alkanedithol chain is placed between two leads of gold with 2160 atoms each. The system is placed in a simulation box with periodic boundaries that has the x, y dimensions conform to the edges of Au leads, but a substantial height in the z dimension, with the top of the box placed far from the atoms.

The atom types comprise of Au, S, and CH2. For this model, C and H are grouped into an united CH2 atom due to negligible contribution to thermal transport by interactions from the C-H bond. Henceforth, C atoms will refer to united CH₂ atoms. We display in Fig. 10 our assignment of different atom types (1-6), as well as defined sections (1–30) for which temperature data will be collected. Note that we distinguish between four different Au atom (types 1–4) since they are handled differently in simulations, as we now explain. Each Au section consists of 270 atoms (separated into sections with 180 and 90 atoms at the very ends). The individual S and C atoms on the molecule also define sections, giving a total of 30 sections for a 10-unit S-alkane-S chain. The total number of Au atoms in sections 3-9 is 1890, thus we have 3780 Au atoms in both leads. Our standard setup consists of seven sections of Au at each contact, for which temperature data are collected.

As shown in Fig. 10, atoms type 1 exist on both ends of the leads as a fixed Au that holds the rest of the lead in place to prevent collapsing. These atoms are not allowed to move in simulations and their role is to hold the junction and prevent the gold pieces from collapsing onto one another. Atom types 2 and 3 are single

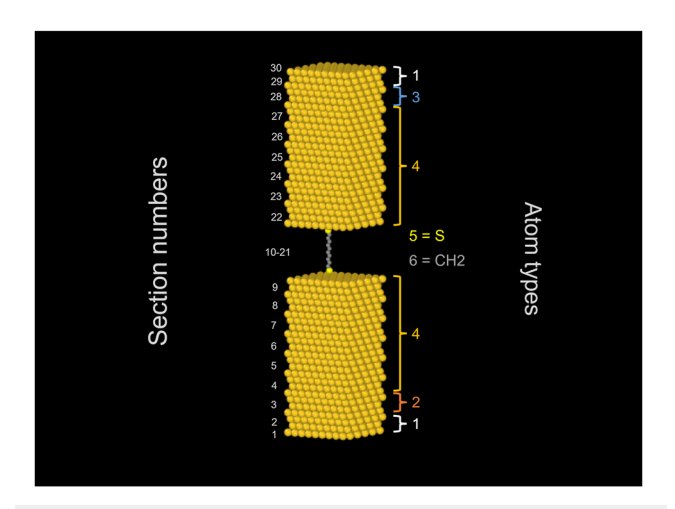


FIG. 10. Visualization of the initial coordinate file (OVITO⁷⁸) used in RNEMD simulations for $N_C = 10$. We list atom types (1–6) and section numbers (1–30), with the temperature profile evaluated for each section (barring the boundaries, type 1).

sections of Au, where heat is inputted and outputted, respectively. The rest of the moving Au is grouped as type 4. Atom types 5 and 6 correspond to S and C, respectively, where we use the united atom description.

The force field and its parameters are described in Table II; it was adopted from Ref. 73. Intermolecular potentials were adopted from simulations on nanocrystal arrays⁷³ and SAMs.^{24,25} Interactions within the alkanedithiol molecule are approximated by harmonic two- and three-body interactions, as well as four-body (dihedral) interactions. The Morse potential governs the interaction between the metal and the molecule, namely the Au and S interaction. Au-Au interactions are given by the embedded atom model (EAM). 74,75 A Lennard-Jones potential is set for long-range, non-bonded interaction between all atoms.

2. Equilibration

NPT equilibration is carried out first to relax the system, barostatting for zero pressure and to a target temperature. NVT propagation is subsequently carried out by equilibrating the entire system to T = 300 K. Each equilibration is carried over 1.5 ns with 1 fs timesteps.

3. Production run

After equilibration, we carry out long production runs with NVE simulations to produce temperature profiles in a steady state. At this stage, heat is inputted and extracted (as kinetic energy per unit time to the atoms) at the same rate to and from atom types 2 and 3, respectively. It was determined that a heat current (*J*) on the order of 0.01-0.04 eV/ps produces temperature differences of order 50-200 K. Production runs are executed for a total of 22.5 ns, with results being averaged over the last 20 ns. Raw temperature data are collected by logging every 1000 steps of 1 fs timesteps, equivalent to every 1 ps.

APPENDIX B: IMPLEMENTATION OF AEMD SIMULATIONS

In this appendix, we describe the implementation of the AEMD simulation method.

1. Setup

The initial, rigid structure of the system is displayed in Fig. 11, where a single alkanedithol chain is placed between two leads of gold with 2160 atoms each. Similar to RNEMD, the system has periodic boundaries in the x and y dimensions (planes of gold), but the box is extended in the z dimension; the top of the box is placed further away from the atoms.

Similar to Appendix A, atom types comprise of Au, S, and CH₂. As shown in Fig. 11, atom type 1 exists on both ends of the leads as the fixed Au that holds the rest of the lead in place to prevent collapsing. Atoms types 2 and 3 designate the moving Au of their respective leads, which will be equilibrated to high and low temperatures. Types

TABLE II. List of potentials and interactions used in MD simulations. Parameters were adopted from Ref. 73.

Potential	Interaction	Parameters
Harmonic - stretching $E_s = \frac{1}{2}k_s(r - r_0)^2$	C-C S-C	$k_s = 11.27 \text{ eV/Å}^2, r_0 = 1.54 \text{ Å}$ $k_s = 9.627 \text{ eV/Å}^2, r_0 = 1.815 \text{ Å}$
$\frac{L_{s}-\frac{1}{2}\kappa_{s}(r-r_{0})}{r}$	3-6	K _S = 9.027 EV/A , I ₀ = 1.013 A
Harmonic-bending	C-C-C	$k_{\theta} = 5.388 \text{ eV/rad}^2, \theta_0 = 109.5^{\circ}$
$E_{\theta} = \frac{1}{2}k_{\theta}(\theta - \theta_0)^2$	S-C-C	$k_{\theta} = 5.388 \text{ eV/rad}^2, \theta_0 = 114.4^{\circ}$
Dihedral	C-C-C-C	$a_0 = 0.096 17 \text{eV}$
	S-C-C-C	$a_1 = -0.125988\mathrm{eV}$
_		$a_2 = -0.13598 \text{ eV}$
$E_d = \sum_{n=0}^5 a_n \cos^n \phi$	(Same parameters)	$a_3 = 0.0317 \text{ eV}$
	(sume parameters)	$a_4 = 0.27196 \mathrm{eV}$
		$a_5 = 0.32642 \text{ eV}$
Morse		$D_e = 0.38 \text{ eV}$
$E_M = D_e [e^{-2\alpha(r-r_0)} - 2e^{-\alpha(r-r_0)}]$	Au-S	$\alpha = 1.47 \text{ Å}^{-1}$
$E_M = D_e[e^{-i\omega t} - 2e^{-i\omega t}]$		$r_0=2.65~\mathrm{\AA}$
Embedded atom model	Au-Au	Reference 74
Embedded atom model	Ag-Ag, Au-Ag	Reference 75
Lennard-Jones	Au and Au	$\varepsilon = 0.001 69 \text{eV}, \sigma = 2.935 \text{Å}$
$E_{LJ} = 4 \varepsilon_{ij} \left[\left(rac{\sigma_{ij}}{r_{ij}} ight)^{12} - \left(rac{\sigma_{ij}}{r_{ij}} ight)^6 ight]$ with Lorentz–Berthelot mixing rules	Au and C	$\varepsilon = 0.00294 \text{ eV}, \sigma = 3.42 \text{ Å}$
$EL_J = 4\epsilon_{ij} \left[\left(\frac{r_{ij}}{r_{ij}} \right) - \left(\frac{r_{ij}}{r_{ij}} \right) \right]$ with Lorentz-Berthelot mixing rules	S and S	$\varepsilon = 0.017 24 \text{eV}, \sigma = 4.25 \text{Å}$
$\varepsilon_{ij} = \sqrt{\varepsilon_i \varepsilon_j}, \ \sigma_{ij} = \frac{1}{2} (\sigma_i + \sigma_j)$	S and C	$\varepsilon = 0.01086\text{eV},\sigma = 3.55\text{Å}$
where i, j denote different atom types	C and C	$\varepsilon = 0.005 \ 12 \ \text{eV}, \ \sigma = 3.905 \ \text{Å}$

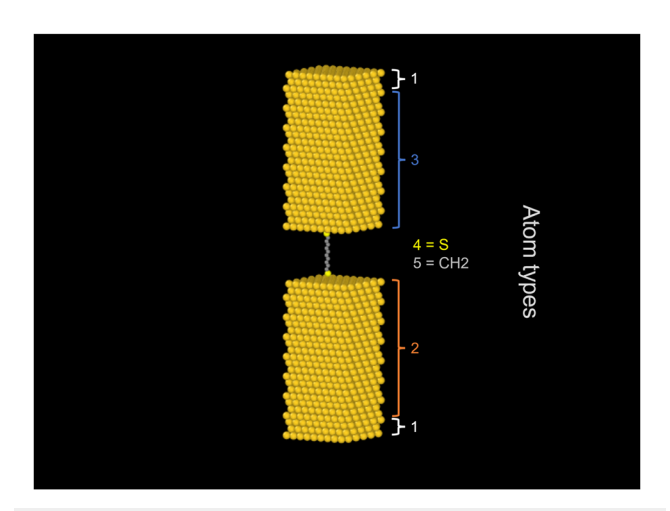


FIG. 11. Visualization of AEMD initial coordinate file (OVITO) for $N_{\rm C}=10$, with listed atom types used for simulation.

4 and 5 are S and C atoms, respectively. The force field used was the same as in the RNEMD.

2. Equilibration

NPT equilibration is carried out first to relax the system and simulation box, barostatting for zero pressure and thermostatting to a target temperature, \bar{T} . Subsequent NVT equilibration is carried out individually on the two Au leads to T_h and T_c , where $\bar{T} = \frac{1}{2} (T_h + T_c)$. Equilibration steps are carried out over 1.5 ns with 1 fs timesteps.

3. Production run

The two leads are connected via the molecule. An NVE simulation is conducted on the overall system for a total simulation time of 5 ns. During this time, the temperatures of the Au lead relax to the equilibrium value, \bar{T} . Raw temperature data are collected by logging every 1000 steps of 1 fs timesteps, equivalent to every 1 ps.

APPENDIX C: FORCE FIELD: POTENTIALS AND PARAMETERS

Table II shows list of potentials and interactions used in MD simulations.

APPENDIX D: HEAT TRANSPORT IN M-MOLECULE-M' JUNCTIONS: LANDAUER FORMALISM

We complement here the MD results presented in Fig. 9 using a minimal model for thermal transport. Our goal is to demonstrate the effect of Debye frequencies of the attached metals (or more generally, their phonon spectra) on the phonon heat current. Using the quantum Landauer formula for phonon heat transport, we study here heat transport in M-alkanedithiol-M' junctions with the metals being either Au or Ag. Consistent with Fig. 9, we find that around room temperature, Ag, which has a higher Debye frequency than Au, supports higher currents for the same thermal bias. Mismatched

junctions, however, show in the harmonic model conductance values close to the case of gold, unlike MD simulations that bring values between the same-metal junctions.

In our minimal model, the molecule is represented by a single harmonic mode of frequency ω_0 . We assume Ohmic functions for the two phonon baths, albeit we use different Debye temperatures for Au and Ag. To restrict the comparison to the difference in Debye frequencies, we normalize the heights of the two spectral functions so that they match at their maximum value.

For a fully harmonic model, the phonon heat current is given by a Landauer-type expression. ⁷⁶ Considering a single-mode system, a calculation of the transmission function yields ^{10,39}

$$J = \frac{2}{\pi} \int_{-\infty}^{\infty} d\omega \hbar \omega \frac{\omega^2 \gamma_{\rm M}(\omega) \gamma_{\rm M'}(\omega)}{(\omega^2 - \omega_0^2)^2 + \omega^2 (\gamma_{\rm M}(\omega) + \gamma_{\rm M'}(\omega))^2} \times [n_{\rm M}(\omega) - n_{\rm M'}(\omega)]. \tag{D1}$$

Here, $n_{\rm M}(\omega)$ is the Bose–Einstein distribution function evaluated at the temperature of the M metal. We used a spectral density function with a hard cutoff: $\gamma_M(\omega) = C_M \omega e^{-\omega/\omega_M}$ for $\omega \leq \omega_M$ and $\gamma_M(\omega) = 0$ for $\omega > \omega_M$. The spectral density function is related to the phonon density of states. We used a function with a hard cutoff to reflect the absence of phonon modes in the metal beyond a certain frequency. We tested in simulations other forms for the spectral density function (e.g., ignoring the exponential factor); we found those results to be similar to what we present next. C_M is a dimensionless constant controlling the metal-molecule coupling strengths. ω_M is the Debye frequency of the M metal. The two spectral functions are presented in Fig. 12(a). Since $\omega_{\rm Ag} > \omega_{\rm Au}$, the phonon spectra of Ag are displaced to higher frequencies.

Our results for the heat current are presented in Figs. 12(b) and 12(c). Since we take into account a single molecular mode, we study the current as a function of the molecular frequency ω_0 . The behavior of the current is monotonic with ω_0 , thus the overall trends are expected to hold even when multiple modes contribute.

Around room temperature, according to Fig. 12(b), Ag junctions support the highest currents while Au junctions show a lower current. The mismatched case supports a current close to the value of gold's junctions. Results for the homogeneous junctions qualitatively agree with and support RNEMD simulations as presented in Fig. 9. This behavior can be rationalized based on the higher spectral density of Ag metal compared with Ag around room temperature, 0.025 eV.

To decouple our model harmonic effects from quantum statistics, we had further tested the behavior of currents when we replace the quantum baths with classical ones. That is, we replace the Bose–Einstein distribution functions with their classical-high temperature limits. Our results were essentially unchanged by going to the classical limit.

As for a quantitative comparison between the minimal-model calculation and classical MD simulations: Given the significant simplifications in the minimal model here (single molecular mode, fully harmonic force field) we do not expect the numbers to agree. However, we note that according to the MD study the conductance of Ag junctions is about 40% higher than Au, see Fig. 9. The single-model provides smaller ratios, with $G_{\rm Ag-Ag}/G_{\rm Au-Au} \approx 1.2$, see Fig. 12(b).

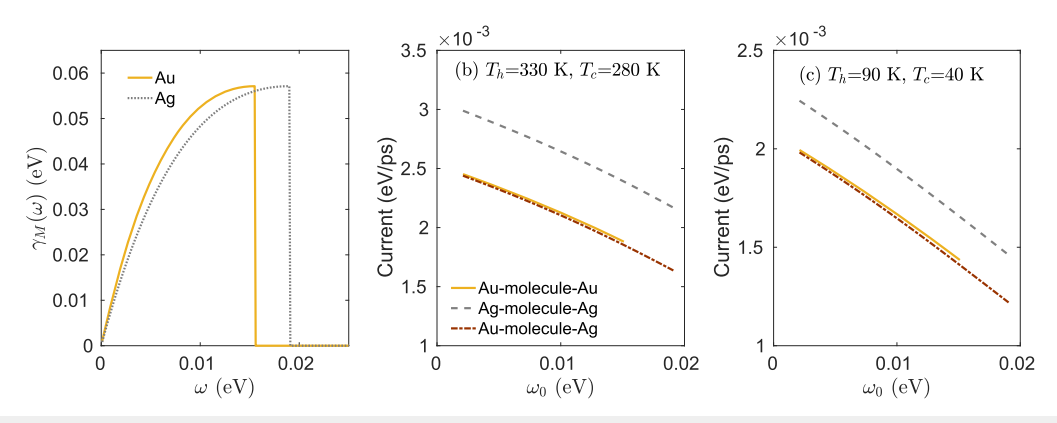


FIG. 12. Analysis of phonon heat transport in M-alkanedithiol-M' junctions using a single-mode harmonic model. (a) Phononic spectral density functions $\gamma_{\rm M}(\omega)$ used to describe M = Au, Ag, differing by their Debye frequencies, $T_D^{\rm Au}=180$ K and $T_D^{\rm Ag}=220$ K, and normalized by height. (b) Heat current for gold, silver, and mismatched junctions for $T_h=340$ K, $T_c=270$ K and at (c) lower temperatures, $T_h=90$ K, $T_c=40$ K. We used the constants $C_{\rm Au}=10$ and $C_{\rm Ag}=0.8C_{\rm Au}$ in the spectral density function $\gamma_{\rm M}(\omega)$, so as to reach the same maximal value in panel (a).

The parameter C_M in the spectral density function $\gamma_M(\omega)$ determines the strength of the metal-molecule coupling, with the measure for the interaction energy $E_R = C_M \omega_M$. This can be regarded as a reorganization energy for phonon transport from the metals to the system. The Debye frequencies for Au and Ag are in the 20 meV range, thus a reasonable value for C_M would be at 10, arriving at a metal-molecule coupling energy of 0.2 eV. In Fig. 13, we show that the current slowly varies with this coupling energy. Therefore, the specific choice of C_M does not affect our conclusions.

Altogether, the simple harmonic model provides predictions in line with MD simulations for homogeneous chains. In contrast,

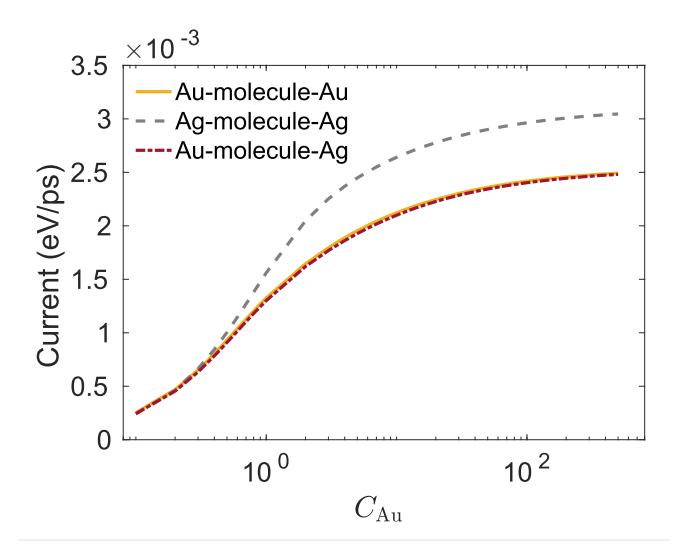


FIG. 13. Analysis of phonon heat transport in M-alkanedithiol-M' junctions based on a single-mode model, displaying the dependence of the heat current on the coupling parameter $C_{\rm Au}$. $T_h=340$ K, $T_c=270$ K and we set $C_{\rm Ag}=0.8C_{\rm Au}$, see Fig. 12.

to understand transport in mismatched Au-molecule-Ag junctions, one needs to include anharmonic effects. In mismatched junctions, the contribution of anharmonic interactions is significant, allowing transport, e.g., from the tail of the Ag spectral function $(\omega_{\rm Au} < \omega < \omega_{\rm Ag})$ to Au.

REFERENCES

¹E. Pop, "Energy dissipation and transport in nanoscale devices," Nano Res. 3, 147 (2010).

²N. Li, J. Ren, L. Wang, G. Zhang, P. Hänggi, and B. Li, "*Colloquium*: Phononics: Manipulating heat flow with electronic analogs and beyond," Rev. Mod. Phys. **84**, 1045 (2012).

⁵T. Luo and G. Chen, "Nanoscale heat transfer - from computation to experiment," Phys. Chem. Chem. Phys. 15, 3389 (2013).

⁴D. G. Cahill, P. V. Braun, G. Chen, D. R. Clarke, S. Fan, K. E. Goodson, P. Keblinski, W. P. King, G. D. Mahan, A. Majumdar, H. J. Maris, S. R. Phillpot, E. Pop, and L. Shi, "Nanoscale thermal transport. II. 2003–2012," Appl. Phys. Rev. 1, 011305 (2014).

⁵D. M. Leitner, "Quantum ergodicity and energy flow in molecules," Adv. Phys. **64**, 445 (2015).

⁶D. Segal and B. K. Agarwalla, "Vibrational heat transport in molecular junctions," Annu. Rev. Phys. Chem. **67**, 185 (2016).

⁷S. Park, J. Jang, H. Kim, D. I. Park, K. Kim, and H. J. Yoon, "Thermal conductance in single molecules and self-assembled monolayers: Physicochemical insights, progress, and challenges," J. Mater. Chem. A 8, 19746 (2020).

⁸Y. Li, W. Li, T. Han, X. Zheng, J. Li, B. Li, S. Fan, and C.-W. Qiu, "Transforming heat transfer with thermal metamaterials and devices," Nat. Rev. Mater. **6**, 488 (2021).

⁹B. Gotsmann, A. Gemma, and D. Segal, "Quantum phonon transport through channels and molecules—A perspective," Appl. Phys. Lett. **120**, 160503 (2022).

¹⁰D. Segal, A. Nitzan, and P. Hänggi, "Thermal conductance through molecular wires," J. Chem. Phys. **119**, 6840 (2003).

¹¹K. Sasikumar and P. Keblinski, "Effect of chain conformation in the phonon transport across a Si-polyethylene single-molecule covalent junction," J. Appl. Phys. 109, 114307 (2011).

¹²J. C. Klöckner, M. Bürkle, J. C. Cuevas, and F. Pauly, "Length dependence of the thermal conductance of alkane-based single-molecule junctions: An *ab initio* study," Phys. Rev. B **94**, 205425 (2016).

- ¹³J. C. Klöckner, J. C. Cuevas, and F. Pauly, "Transmission eigenchannels for coherent phonon transport," Phys. Rev. B 97, 155432 (2018).
- ¹⁴R. Moghaddasi Fereidani and D. Segal, "Phononic heat transport in molecular junctions: Quantum effects and vibrational mismatch," J. Chem. Phys. 150, 024105 (2019).
- ¹⁵I. Sharony, R. Chen, and A. Nitzan, "Stochastic simulation of nonequilibrium heat conduction in extended molecular junctions," J. Chem. Phys. 153, 144113 (2020).
- ¹⁶G. Li, B.-Z. Hu, N. Yang, and J.-T. Lü, "Temperature-dependent thermal transport of single molecular junctions from semiclassical Langevin molecular dynamics," Phys. Rev. B 104, 245413 (2021).
- ¹/₂M. Dinpajooh and A. Nitzan, "Heat conduction in polymer chains: Effect of substrate on the thermal conductance," J. Chem. Phys. **156**, 144901 (2022).
- ¹⁸L. Cui, S. Hur, Z. A. Akbar, J. C. Klöckner, W. Jeong, F. Pauly, S.-Y. Jang, P. Reddy, and E. Meyhofer, "Thermal conductance of single-molecule junctions," Nature 572, 628 (2019).
- ¹⁹N. Mosso, H. Sadeghi, A. Gemma, S. Sangtarash, U. Drechsler, C. Lambert, and B. Gotsmann, "Thermal transport through single-molecule junctions," Nano Lett. **19**, 7614 (2019).
- ²⁰R. Y. Wang, R. A. Segalman, and A. Majumdar, "Room temperature thermal conductance of alkanedithiol self-assembled monolayers," Appl. Phys. Lett. 89, 173113 (2006).
- ²¹ Z. Wang, J. A. Carter, A. Lagutchev, Y. K. Koh, N.-H. Seong, D. G. Cahill, and D. D. Dlott, "Ultrafast flash thermal conductance of molecular chains," Science 317, 787 (2007).
- M. D. Losego, M. E. Grady, N. R. Sottos, D. G. Cahill, and P. V. Braun, "Effects of chemical bonding on heat transport across interfaces," Nat. Mater. 11, 502 (2012).
 T. Meier, F. Menges, P. Nirmalraj, H. Hölscher, H. Riel, and B. Gotsmann, "Length-dependent thermal transport along molecular chains," Phys. Rev. Lett. 113, 060801 (2014).
- ²⁴S. Majumdar, J. A. Sierra-Suarez, S. N. Schiffres, W.-L. Ong, C. F. Higgs III, A. J. H. McGaughey, and J. A. Malen, "Vibrational mismatch of metal leads controls thermal conductance of self-assembled monolayer junctions," Nano Lett. 15, 2985 (2015)
- ²⁵S. Majumdar, J. A. Malen, and A. J. H. McGaughey, "Cooperative molecular behavior enhances the thermal conductance of binary self-assembled monolayer junctions," Nano Lett. **17**, 220 (2017).
- ²⁶T. Luo and J. R. Lloyd, "Non-equilibrium molecular dynamics study of thermal energy transport in Au–SAM–Au junctions," Int. J. Heat Mass Transfer **53**, 1 (2010).
- ²⁷L. Hu, L. Zhang, M. Hu, J.-S. Wang, B. Li, and P. Keblinski, "Phonon interference at self-assembled monolayer interfaces: Molecular dynamics simulations," Phys. Rev. B 81, 235427 (2010).
- ²⁸G. Kikugawa, T. Ohara, T. Kawaguchi, I. Kinefuchi, and Y. Matsumoto, "A molecular dynamics study on heat conduction characteristics inside the alkanethiolate SAM and alkane liquid," Int. J. Heat Mass Transfer 78, 630 (2014).
- ²⁹Y. Wang, Y. Cao, K. Zhou, and Z. Xu, "Assessment of self-assembled monolayers as high-performance thermal interface materials," Adv. Mater. Interfaces **4**, 1700355 (2017)
- ³⁰ J.-S. Wang, B. K. Agarwalla, H. Li, and J. Thingna, "Nonequilibrium Green's function method for quantum thermal transport," Front. Phys. 9, 673 (2014).
- ³¹ Y.-J. Zeng, Z.-K. Ding, H. Pan, Y.-X. Feng, and K.-Q. Chen, "Nonequilibrium Green's function method for phonon heat transport in quantum system," J. Phys.: Condens. Matter 34, 223001 (2022).
- ³²A. P. Thompson, H. M. Aktulga, R. Berger, D. S. Bolintineanu, W. M. Brown, P. S. Crozier, P. J. in 't Veld, A. Kohlmeyer, S. G. Moore, T. D. Nguyen, R. Shan, M. J. Stevens, J. Tranchida, C. Trott, and S. J. Plimpton, "LAMMPS—A flexible simulation tool for particle-based materials modeling at the atomic, meso, and continuum scales," Comput. Phys. Commun. 271, 108171 (2022).
- ³³T.-Q. Duong, C. Massobrio, G. Ori, M. Boero, and E. Martin, "Thermal resistance of an interfacial molecular layer by first-principles molecular dynamics," J. Chem. Phys. **153**, 074704 (2020).
- ³⁴N. A. Roberts and D. G. Walker, "A review of thermal rectification observations and models in solid materials," Int. J. Therm. Sci. 50, 648 (2011).

- ³⁵G. Wehmeyer, T. Yabuki, C. Monachon, J. Wu, and C. Dames, "Thermal diodes, regulators, and switches: Physical mechanisms and potential applications," Appl. Phys. Rev. 4, 041304 (2017).
- ³⁶M. Terraneo, M. Peyrard, and G. Casati, "Controlling the energy flow in non-linear lattices: A model for a thermal rectifier," Phys. Rev. Lett. **88**, 094302 (2002).
- ³⁷B. Li, L. Wang, and G. Casati, "Thermal diode: Rectification of heat flux," Phys. Rev. Lett. 93, 184301 (2004).
- ³⁸B. Hu, L. Yang, and Y. Zhang, "Asymmetric heat conduction in nonlinear lattices," Phys. Rev. Lett. 97, 124302 (2006).
- ³⁹D. Segal and A. Nitzan, "Spin-boson thermal rectifier," Phys. Rev. Lett. 94, 034301 (2005).
- ⁴⁰ L. A. Wu, C. X. Yu, and D. Segal, "Nonlinear quantum heat transfer in hybrid structures: Sufficient conditions for thermal rectification," Phys. Rev. E 80, 041103 (2009).
- ⁴¹ Z. Li, S. Xiong, C. Sievers, Y. Hu, Z. Fan, N. Wei, H. Bao, S. Chen, D. Donadio, and T. Ala-Nissila, "Influence of thermostatting on nonequilibrium molecular dynamics simulations of heat conduction in solids," J. Chem. Phys. **151**, 234105 (2019)
- ⁴²Z. Rieder, J. L. Lebowitz, and E. Lieb, "Properties of a harmonic crystal in a stationary nonequilibrium state," J. Math. Phys. **8**, 1073 (1967).
- ⁴³J. Chen, X. Xu, J. Zhou, and B. Li, "Interfacial thermal resistance: Past, present, and future," Rev. Mod. Phys. **94**, 025002 (2022).
- ⁴⁴G. Wu and B. Li, "Thermal rectification in carbon nanotube intramolecular junctions: Molecular dynamics calculations," Phys. Rev. B **76**, 085424 (2007).
- ⁴⁵G. Wu and B. Li, "Thermal rectifiers from deformed carbon nanohorns," J. Phys.: Condens. Matter **20**, 175211 (2008).
- ⁴⁶M. Hu, P. Keblinski, and B. Li, "Thermal rectification at silicon-amorphous polyethylene interface," Appl. Phys. Lett. **92**, 211908 (2008).
- ⁴⁷N. Yang, G. Zhang, and B. Li, "Carbon nanocone: A promising thermal rectifier," Appl. Phys. Lett. **93**, 243111 (2008).
- ⁴⁸N. Yang, G. Zhang, and B. Li, "Thermal rectification in asymmetric graphene ribbons," Appl. Phys. Lett. **95**, 033107 (2009).
- ⁴⁹L. Zhang, J.-T. Lü, J.-S. Wang, and B. Li, "Thermal transport across metal-insulator interface via electron-phonon interaction," J. Phys.: Condens. Matter 25, 445801 (2013).
- ⁵⁰ D. Segal, "Single mode heat rectifier: Controlling energy flow between electronic conductors," Phys. Rev. Lett. **100**, 105901 (2008).
- ⁵¹F. Giazotto and F. S. Bergeret, "Thermal rectification of electrons in hybrid normal metal-superconductor nanojunctions," Appl. Phys. Lett. **103**, 242602 (2013).
- ⁵² E. Nefzaoui, K. Joulain, J. Drevillon, and Y. Ezzahri, "Radiative thermal rectification using superconducting materials," Appl. Phys. Lett. **104**, 103905 (2014)
- ⁵³P. Ben-Abdallah and S.-A. Biehs, "Phase-change radiative thermal diode," Appl. Phys. Lett. **103**, 191907 (2013).
- ⁵⁴E. Pallecchi, Z. Chen, G. E. Fernandes, Y. Wan, J. H. Kim, and J. Xu, "A thermal diode and novel implementation in a phase-change material," Mater. Horiz. **2**, 125 (2015)
- ⁵⁵ A. Fiorino, D. Thompson, L. Zhu, R. Mittapally, S.-A. Biehs, O. Bezencenet, N. El-Bondry, S. Bansropun, P. Ben-Abdallah, E. Meyhofer, and P. Reddy, "A thermal diode based on nanoscale thermal radiation," ACS Nano 12, 5774 (2018).
- ⁵⁶B. C. Pein, Y. Sun, and D. D. Dlott, "Unidirectional vibrational energy flow in nitrobenzene," J. Phys. Chem. A **117**, 6066 (2013).
- ⁵⁷B. C. Pein, Y. Sun, and D. D. Dlott, "Controlling vibrational energy flow in liquid alkylbenzenes," J. Phys. Chem. B 117, 10898 (2013).
- ⁵⁸ A. J. Schmitz, H. D. Pandey, F. Chalyavi, T. Shi, E. E. Fenlon, S. H. Brewer, D. M. Leitner, and M. J. Tucker, "Tuning molecular vibrational energy flow within an aromatic scaffold via anharmonic coupling," J. Phys. Chem. A 123, 10571 (2019).
- ⁵⁹ K. M. Reid, H. D. Pandey, and D. M. Leitner, "Elastic and inelastic contributions to thermal transport between chemical groups and thermal rectification in molecules," J. Phys. Chem. C **123**, 6256 (2019).

- ⁶⁰D. Segal, "Absence of thermal rectification in asymmetric harmonic chains with self-consistent reservoirs," Phys. Rev. E 79, 012103 (2009).
- ⁶¹ N. I. Rubtsova, L. N. Qasim, A. A. Kurnosov, A. L. Burin, and I. V. Rubtsov, "Ballistic energy transport in oligomers," Acc. Chem. Res. 48, 2547 (2015).
- ⁶²Q. Li, M. Strange, I. Duchemin, D. Donadio, and G. C. Solomon, "A strategy to suppress phonon transport in molecular junctions using π -stacked systems," J. Phys. Chem. C **121**, 7175 (2017).
- ⁶³ M. D. Noori, S. Sangtarash, and H. Sadeghi, "The effect of anchor group on the phonon thermal conductance of single molecule junctions," Appl. Sci. 11, 1066 (2021).
- ⁶⁴D. Schwarzer, P. Kutne, C. Schröder, and J. Troe, "Intramolecular vibrational energy redistribution in bridged azulene-anthracene compounds: Ballistic energy transport through molecular chains," J. Chem. Phys. 121, 1754 (2004).
- ⁶⁵I. V. Rubtsov and A. L. Burin, "Ballistic and diffusive vibrational energy transport in molecules," J. Chem. Phys. 150, 020901 (2019).
- ⁶⁶T. X. Leong, L. N. Qasim, R. T. Mackin, Y. Du, R. A. Pascal, Jr., and I. V. Rubtsov, "Unidirectional coherent energy transport via conjugated oligo(*p*-phenylene) chains," J. Chem. Phys. **154**, 134304 (2021).
- ⁶⁷ A. Maitra, S. Sarkar, D. M. Leitner, and J. M. Dawlaty, "Electric fields influence intramolecular vibrational energy relaxation and line widths," J. Phys. Chem. Lett. **12**, 7818 (2021).
- ⁶⁸Q. Li, I. Duchemin, S. Xiong, G. C. Solomon, and D. Donadio, "Mechanical tuning of thermal transport in a molecular junction," J. Phys. Chem. C 119, 24636 (2015).

- ⁶⁹ J. C. Klöckner, J. C. Cuevas, and F. Pauly, "Tuning the thermal conductance of molecular junctions with interference effects," Phys. Rev. B 96, 245419 (2017).
- ⁷⁰H. Sadeghi, "Quantum and phonon interference-enhanced molecular-scale thermoelectricity," J. Phys. Chem. C 123, 12556 (2019).
- ⁷¹ R. Chen, I. Sharony, and A. Nitzan, "Local atomic heat currents and classical interference in single-molecule heat conduction," J. Phys. Chem. Lett. 11, 4261 (2020).
- ⁷²P. Carpio-Martínez and G. Hanna, "Quantum bath effects on nonequilibrium heat transport in model molecular junctions," J. Chem. Phys. **154**, 094108 (2021).
- ⁷³ W.-L. Ong, S. Majumdar, J. A. Malen, and A. J. H. McGaughey, "Coupling of organic and inorganic vibrational states and their thermal transport in nanocrystal arrays," J. Phys. Chem. C 118, 7288 (2014).
- ⁷⁴G. Grochola, S. P. Russo, and I. K. Snook, "On fitting a gold embedded atom method potential using the force matching method," J. Chem. Phys. **123**, 204719 (2005)
- ⁷⁵X. W. Zhou, R. A. Johnson, and H. N. G. Wadley, "Misfit-energy-increasing dislocations in vapor-deposited CoFe/NiFe multilayers," Phys. Rev. B **69**, 144113 (2004).
- ⁷⁶A. Dhar, "Heat transport in low-dimensional systems," Adv. Phys. 57, 457 (2008).
- ⁷⁷L. Nicolin and D. Segal, "Non-equilibrium spin-boson model: Counting statistics and the heat exchange fluctuation theorem," J. Chem. Phys. 135, 164106 (2011).
- ⁷⁸A. Stukowski, "Visualization and analysis of atomic simulation data with OVITO-the Open Visualization Tool," <u>Mater. Sci. Eng.</u> 18, 015012 (2010).